PHARMACIA

Pharmacia 71: 1–10
DOI 10.3897/pharmacia.71.e127845

Research Article

Prediction of ADMET, molecular docking, DFT, and QSPR of potential phytoconstituents from *Ambrosia maritima* L. targeting xanthine oxidase

Wadah Osman[1,2], Shaza Shantier[3], Nazik Mohamed[2], Sahar Abdalla[4,5], Mona Mohamed[2], Yunsua Umar[6], Asmaa E. Sherif[1,7], Khaled M. Elamin[8], Ahmed Ashour[1,7]

1 *Department of Pharmacognosy, Faculty of Pharmacy, Prince Sattam Bin Abdulaziz University, Al-kharj 11942, Saudi Arabia*
2 *Department of Pharmacognosy, Faculty of Pharmacy, University of Khartoum, P.O. Box 1996, Khartoum, Sudan*
3 *Department of Pharmaceutical Chemistry, Faculty of Pharmacy, University of Khartoum, P.O. Box 1996, Khartoum, Sudan*
4 *Chemistry Department, College of Science, Imam Mohammad Ibn Saud Islamic University (IMSIU), Riyadh 11623, Saudi Arabia*
5 *Department of Chemistry, Faculty of Science, University of Khartoum, P.O. Box 321, 11115 Khartoum, Sudan*
6 *Department of Chemical and Process Engineering Technology, P.O. Box 10099, Julian Industrial City, Saudi Arabia*
7 *Department of Pharmacognosy, Faculty of Pharmacy, Mansoura University, Mansoura 35516, Egypt*
8 *Graduate School of Pharmaceutical Sciences, Kumamoto University, 5-1 Oe-honmachi, Chuo-ku, Kumamoto 862-0973, Japan*

Corresponding author: Wadah Osman (W.osman@psau.edu.sa)

Received 9 June 2024 ♦ **Accepted** 9 July 2024 ♦ **Published** 30 July 2024

Citation: Osman W, Shantier S, Mohamed N, Abdalla S, Mohamed M, Umar Y, Sherif AE, Elamin KM, Ashour A (2024) Prediction of ADMET, molecular docking, DFT, and QSPR of potential phytoconstituents from *Ambrosia maritima* L. targeting xanthine oxidase. Pharmacia 71: 1–10. https://doi.org/10.3897/pharmacia.71.e127845

Abstract

This study aimed to evaluate the xanthine oxidase (XO) inhibitory activities of seven compounds identified in the potent antioxidant ethyl acetate fraction of *Ambrosia maritima* L. using various computational tools. Physicochemical properties and density functional theory (DFT) analyses were performed. Subsequently, XO molecular docking was performed to identify the most promising leads. The water solubility of the compounds varied among highly soluble, moderately soluble, and soluble compounds. Four compounds were predicted to have no mutagenic or tumorigenic effect. All compounds were found to have lower binding energies than the oxypurinol standard, indicating their potential as XO inhibitors. The predicted inhibitory interactions, physicochemical properties, and DFT results suggest that two of the compounds (Kaempferol-3-O-glucoside and escululin) are promising drugs or drug leads for the treatment of certain diseases related to increased levels of XO.

Keywords

xanthine oxidase, *Ambrosia maritima* L., ADME properties, DFT, molecular docking, oxypurinol

Introduction

Xanthine oxidase (XO) serves as the crucial enzyme responsible for the degradation of purines, transforming hypoxanthine and xanthine into uric acid and simultaneously generating reactive oxygen species such as H2O2, O2-, and ROS (Dhiman et al. 2013; Nepali et al. 2011). The overproduction of this enzyme leads to a condition known as hyperuricemia, which may result in a range of chronic and acute diseases, including gout,

Copyright *Osman W et al.* This is an open access article distributed under the terms of the Creative Commons Attribution License (CC-BY 4.0), which permits unrestricted use, distribution, and reproduction in any medium, provided the original author and source are credited.

PENSOFT

renal failure, tumor lysis syndrome, coronary heart disease, hematospermia, arterial hypertension, and metabolic syndrome (Xu et al. 2019; Pacher et al. 2006; Mehmood et al. 2019; El-Naeem et al. 2022). Therefore, XO inhibitors are currently attractive therapeutics for disorders such as hyperuricemia and its related diseases, ulcers, cancer, ischemia, diabetes, obesity, hyperlipidemia, hypertension, and oxidative damage (Hediger et al. 2005; Kumar et al. 2011). Despite the availability of XO inhibitor drugs, such as allopurinol and febuxostat, some side effects have been reported, including skin rashes, hepatitis, fever, Stevens-Johnson syndrome, nephropathy, fatal liver necrosis, and allergic reactions (Radi et al. 1997; Spector and Johns 1970; Hosoya et al. 2014; Lu and Yao 2013; Borges et al. 2002). Thus, alternative medicines with fewer adverse effects are necessary. Due to their beneficial activities and fewer side effects, natural products play a crucial role in innovative drug discovery by providing structural leads for the development of new therapeutic agents against various diseases (Mehmood et al. 2019).

Ambrosia maritima L. (family Asteraceae) is a plant distributed in the Mediterranean region of African countries, particularly Egypt and Sudan (Said et al. 2018). Sudanese folk medicine is commonly used to treat various conditions, including cancer, bilharziasis, diabetes, hypertension, kidney stones, asthma, rheumatic pain, and urinary tract infections. When combined with sugar at a ratio of 1:3, it can also be used as an appetizer, aiding digestion, and acting as a tonic (Said et al. 2018; Helal et al. 2014).

Based on the aforementioned reports, this study aimed to evaluate Xanthine Oxidase inhibitory activity and conduct pharmacokinetics and molecular analysis of seven compounds (Fig. 1), which were previously identified from *Ambrosia maritima* L. hydroalcoholic extract (Mohamed et al. 2020), utilizing various in silico and web-based tools.

Materials and methods

ADME properties and physicochemical parameters

The SMILES approach was employed to evaluate the absorption, distribution, metabolism, and excretion (ADME) and Lipinski's rule for five out of the seven compounds. To determine the properties, the pkCSM website (http://biosig.unimelb.edu.au/pkcsm/) was utilized.

Toxicity risk prediction

The Protox II website (http://tox.charite.de/protox_II) was utilized to predict the toxicity of compounds. The toxicity chemical class prediction was categorized into the following six classes: Class 1: extremely lethal (LD50 ≤ 5), Class 2: fatal (5 < LD50 ≤ 50), Class 3: toxic (50 < LD50 ≤ 300), Class 4: harmful (300 < LD50 ≤ 2000), Class 5: possibly hazardous (2000 < LD50 ≤ 5000), and Class 6: non-toxic (LD50 > 5000) (OECD 2001).

Determination of the QSPR

QSPR strives to establish the quantitative correlation between molecular structure and physicochemical properties (Shoombuatong et al. 2017). Physicochemical parameters, including lipophilic, electronic, and steric parameters, were predicted using the Gaussian 09 program suite (Frisch et al. 2009). Lipophilic parameters, including LogP and LogS; electronic parameters, including E_{TOT}, E_{HOMO}, and E_{LUMO}; and steric parameters, including molecular weight (MW) and molecular volume (MV), were calculated. The total clearance (CL_{TOT}) value as a parameter of drug elimination was predicted using online pkCSM (http://biosig.unimelb.edu.au/pkcsm/prediction). The QSPR equation was determined using Microsoft Excel 2013 (https://office.microsoft.com/Excel).

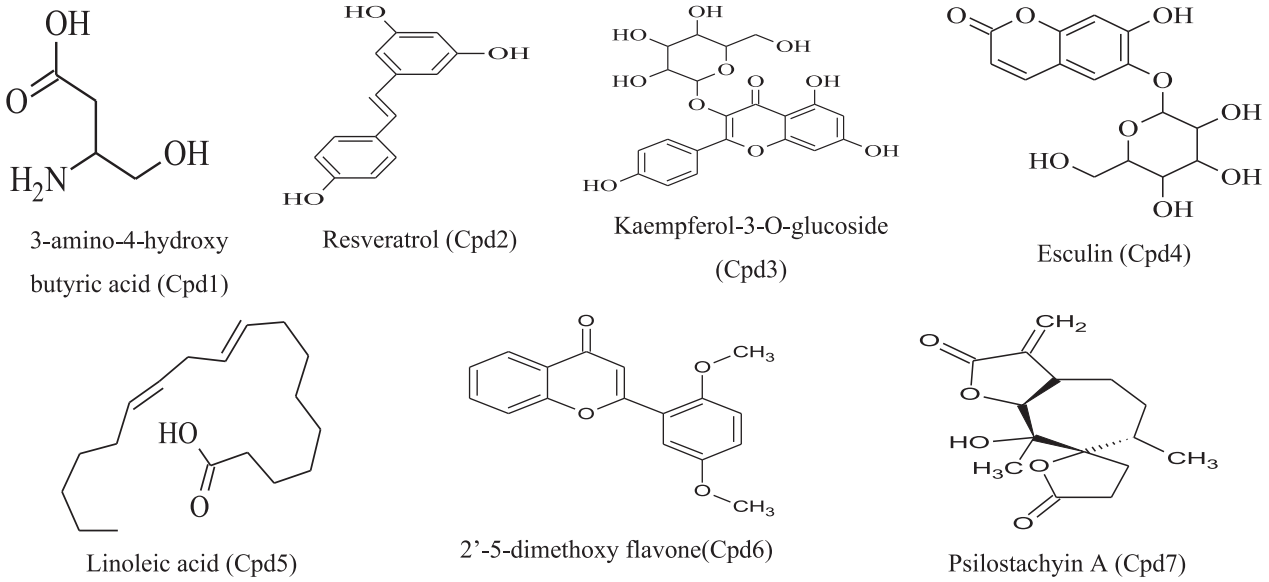

Figure 1. Chemical structures of identified compounds.

Density functional calculations

The Gaussian 09 program suite (Frisch et al. 2009) was used to optimize the molecular structures and compute the total energies, dipole moments, and molecular orbital energies of the molecules (Fig. 1). All calculations were performed using the most popular hybrid density, B3YLP (Becke 1993; Lee et al. 1988; Sousa et al. 2007), along with the 6-31++G (d, p) basis set. The harmonic vibrational frequencies were determined using the same method used for optimization to ensure that all molecules were local minima structures in the absence of imaginary frequencies. Using the HOMO and LUMO energies, several molecular properties were calculated: The HOMO-LUMO energy gap, ionization potential (I), electron affinity (A), chemical hardness (η), molecular softness (S), electronic chemical potential (μ), electronegativity (χ), and electrophilicity index (ω) were calculated.

Molecular docking

Target proteins and prospective ligands have been developed for accurate computational computation. Ligand preparation was performed using the LigPrep tool interfaced with the Maestro module of the Schrödinger suite. Using the optimal potential liquid simulation (OPLS4) force field, the 3D structures of all the ligands and the reference chemical oxypurinol, including all potential tautomers and ionization states at pH 7.0 ± 2.0, were created and reduced. Schrödinger's multi-step Protein Preparation Wizard (PrepWizard) was used for protein preparation. First, the RCSB Protein Data Bank was used to obtain a high-resolution protein crystal structure of XO (PDB: 3NVY) at a resolution of 2 Å, which contains a quercetin molecule in its binding site. The allocation of bond orders and charges was accompanied by the addition of hydrogen atoms to the heavy atoms, while all water molecules and heteroatoms were eliminated, ensuring that quercetin remained in the active site. The OPLS4 force field was employed to optimize and minimize the energy of the final structures for both the ligand and protein. A formal representation of the binding pocket was generated using the centroid of the co-crystallized native ligand (quercetin), with default settings maintained for each case. The Glide XP module of the Schrödinger Suite was utilized to dock the identified compounds and reference standards into the active sites of the crystal structures (Schrodinger 2021).

Quercetin was subsequently docked into the pre-prepared XO binding site to validate the binding site. The molecule's most optimal docked pose was subsequently compared to the conformation of the bound ligand as well as the X-ray crystal orientation, and the root-mean-square deviation (RMSD) was calculated.

Results and discussion

Common plants are a major source of biologically active compounds, which are currently attracting considerable attention. These plants are essential to satisfy basic health needs, particularly in developing countries, according to the World Health Organization (WHO) (Naqvi et al. 1994). The compounds suggested in our present work have been reported to possess antioxidant, antidiabetic, anti-inflammatory, and other properties (Habtemariam 2011; Niu et al. 2015; Wang et al. 2014). Essa et al. studied the xanthine oxidase inhibitory activity of Plumeria rubra flower extracts, in which kaempferol-3-*O*-glucoside was identified as a phytoconstituent (Mohamed et al. 2018). Moreover, Ahmane et al. studied the in vitro and in vivo inhibitory activities of xanthine oxidase by Fraxinus angustifolia extracts, which were found to contain esculin and kaempferol glucoside. These reports support the findings of previous work conducted by Nazik et al. (Mohamed et al. 2020) and consequently suggest the importance of these compounds for further study and investigation in terms of theoretical and geometric analysis, in addition to their binding interactions.

Therefore, the present study focused on the geometric analysis and inhibitory activity evaluation of seven compounds identified in *Ambrosia maritima* L.

ADME properties and physicochemical parameters

Based on the obtained physicochemical and ADME properties, the analyzed compounds showed different water solubilities that varied from very soluble, highly soluble, moderately soluble, and soluble (Table 1), indicating that they are less likely to have solubility problems and thus have good bioavailability (Bergström et al. 2016). Five compounds were found to have high gastrointestinal absorption after oral administration, and five compounds did not permeate the BBB. Only two compounds are P-gp substrates that protect the central nervous system (CNS) from xenobiotics. Cytochrome P450 (CYP) enzymes are responsible for the metabolism of many drugs. Therefore, drug-drug interactions and significant side effects resulting from drug or metabolite buildup are caused by the inhibition of these enzymes (Testa and Kraemer 2007). Therefore, an assessment of the effects of potential drug candidates on these enzymes is essential. Four compounds were predicted to be non-inhibitors of any of the five CYP isoforms (Table 1). The physicochemical properties were calculated using Lipinski's rule of five, which states that molecules with logP 5, molecular weight 500 Da, ten hydrogen bond acceptors, and five hydrogen bond donors are most likely drug-like. Molecular entities with ten rotatable bonds and a total polar surface area of 140 are predicted to exhibit high bioavailability, as indicated by our findings in Table 1. These substances are also anticipated to have molecular weights below 500 Da, which facilitates their movement, dispersion, and absorption compared to heavier molecules (Srimai et al. 2013; Pires et al. 2015).

Table 1. Predicted ADME properties and rules of five of the synthesized compounds.

Properties	Cpd1	Cpd2	Cpd3	Cpd4	Cpd5	Cpd6	Cpd7	Unit
Absorption								
Water solubility	0.803	-3.192	-3.059	-2.902	-5.623	-4.226	-2.75	Numeric (log mol/L)
Caco2 permeability	0.674	1.191	-0.3	0.602	1.569	1.351	0.68	Numeric (log Papp in 10–6 cm/s)
Intestinal absorption (human)	68.3	89.057	63.303	37.775	92.282	98.111	96.973	Numeric (% Absorbed)
Skin Permeability	-2.84	-3.16	-2.735	-2.738	-2.493	-2.384	-3.43	Numeric (log Kp)
P-glycoprotein substrate	No	Yes	Yes	No	No	No	No	Categorical (Yes/No)
P-glycoprotein I inhibitor	No	No	No	No	No	No	No	Categorical (Yes/No)
P-glycoprotein II inhibitor	No	No	No	No	No	Yes	No	Categorical (Yes/No)
Distribution								
VDss (human)	-0.578	-0.136	-0.129	-0.462	-0.597	0.014	0.097	Numeric (log L/kg)
Fraction unbound (human)	0.898	0.184	0.125	0.3	0.048	0.195	0.52	Numeric (Fu)
BBB permeability	-0.675	-0.041	-1.779	-1.466	-0.15	-0.09	-0.276	Numeric (log BB)
CNS permeability	-3.153	-2.098	-4.374	-4.126	-1.6	-1.451	-2.91	Numeric (log PS)
Metabolism								
CYP2D6 substrate	No	No	No	No	Yes	No	No	Categorical (Yes/No)
CYP3A4 substrate	No	No	No	No	Yes	Yes	No	Categorical (Yes/No)
CYP1A2 inhibitior	No	Yes	No	No	Yes	Yes	No	Categorical (Yes/No)
CYP2C19 inhibitior	No	Yes	No	No	No	Yes	No	Categorical (Yes/No)
CYP2C9 inhibitior	No	Yes	No	No	No	No	No	Categorical (Yes/No)
CYP2D6 inhibitior	No	Yes	No	No	No	No	No	Categorical (Yes/No)
CYP3A4 inhibitior	No	Yes	No	No	No	No	No	Categorical (Yes/No)
Excretion								
Total Clearance	0.507	0.169	0.273	0.795	1.936	0.325	1.091	Numeric (log ml/min/kg)
Renal OCT2 substrate	No	No	No	No	No	Yes	No	Categorical (Yes/No)
Lipinski's rule of 5								
MW	119.12	228.24	448.38	340.28	280.45	282.29	280.32	Numeric (g/mol)
NRBs	3	2	4	9	3	3	0	-
NHBAs	4	3	10	10	9	4	5	-
NHBDs	3	3	7	0	5	0	1	-
TPSA (A°2)	83.55	60.69	190.28	134.49	37.30	48.67	72.83	-

Toxicity risks and drug-likeliness

According to the Protox II website and the obtained LCD50 values, only four compounds were predicted to be nontoxic (Table 2).

Density functional theory (DFT) analysis

A theoretical density functional analysis was conducted following the prediction of the ADME properties. The highest occupied molecular orbital (HOMO) energy, E_{HOMO}, is associated with the electron-donating ability of the molecule of interest. Consequently, molecules with higher EHOMO values possess an increased capacity to donate electrons to the unoccupied molecular orbital. The value of the lowest unoccupied molecular orbital (LUMO), ELUMO, is directly proportional to the molecule's capacity to accept electrons. In other words, molecules with lower ELUMO values exhibit a greater propensity for accepting electrons. The significance of the HOMO and LUMO, as well as their respective properties, cannot be overstated when it comes to predicting the most reactive positions in π-electron systems and demonstrating various types of reactions in conjugated systems (Kurt et al. 2011). Furthermore, the HOMO and LUMO energy levels indicate the relative chemical stability and biological activity of the molecules. The difference in energy between the two frontier orbitals, known as the HOMO-LUMO energy gap, can be used to predict the strength and stability of the molecule. Molecules with a smaller HOMO-LUMO energy gap are more polarizable and are typically associated with increased chemical reactivity (Kurt et al. 2011; Gunase Karan et al. 2008). Cpds

Table 2. The toxicity prediction of the isolated compounds.

Compound	Predicted LD50	Predicted toxicity class	Average similarity	Prediction accuracy
3-amino-4-hydroxy butyric acid	923 mg/kg	Class 4	76.3%	69.26%
Resveratrol	1560 mg/kg	Class 4	69.97%	68.07%
Kaempferol-3-O-glucoside	5000 mg/kg	Class 5	95.14%	72.9%
Esculin	4000 mg/kg	Class 5	60.85%	68.07%
Linoleic acid	10000 mg/Kg	Class 6	100%	100%
2'-5-dimethoxy flavone	4000 mg/Kg	Class 5	71.86%	69.26%
Psilostachyin A	502 mg/Kg	Class 4	71.68%	69.26%

3 and 4 have good HOMO-LUMO energy gaps, indicating their stability. Inspection of Table 3 reveals that Cpd2 has the lowest HOMO-LUMO gap among the molecules (3.9484 eV). Qualitative molecular representations of the HOMO and LUMO frontier orbitals and their corresponding energy values, in addition to the HOMO-LUMO gaps of the compounds, are depicted in Fig. 2. The HOMO and LUMO are delocalized over the entire cpd2 molecule. In contrast, the HOMO is delocalized at the conjugated part of the carbon chain of the molecule, whereas the LUMO is localized over the carboxylic group in cpd5. The HOMO and LUMO energies were then used to calculate global chemical reactivity descriptors, such as ionization potential (I), electron affinity (A), chemical hardness (η), molecular softness (S), electronic chemical potential (μ), electronegativity (χ), and electrophilicity index (ω). The results are summarized in Tables 1, 2. As shown in the table, the ionization potential of the studied molecules was in the range of 5.9919–7.5402 eV, with cpd7 and cpd5 having the highest and lowest ionization potentials, respectively. In the case of electron affinity, cpd5 had the lowest value of 0.3891 eV, and cpd4 had the highest value of 2.0708 eV. These values reflect the electron-donating and electron-accepting abilities of these compounds. Cpds5 and 1, which have carboxylic acid functional groups, exhibited higher values of chemical hardness and lower values of chemical softness than the other studied molecules. These compounds contain ionizable functional groups (-COOH) and tend to be in ionic form and weakly polarizable. The remaining compounds (2, 3, 4, 6, and 7) contained hydroxyl group(s) and,

Table 3. Calculated total energies, dipole moments, HOMO and LUMO energies, HOMO-LUMO energy gap, ionization potential (I), electron affinity (A), chemical hardness (η), molecular softness (S), electronic chemical potential (μ), electronegativity (χ), and electrophilicity index (ω) calculated at the B3LYP/6-31++G(d,p) level of theory.

Molecular property	Cpd1	Cpd2	Cpd3	Cpd4	Cpd5	Cpd6	Cpd7
Total energy (Hartree)	-438.3074	-766.4255	-1639.7893	-1258.2925	-855.7169	-957.1655	-959.8226
E_{HOMO} (a.u.)	-0.2412	-0.2042	-0.2106	-0.2330	-0.2424	-0.2202	-0.2771
E_{LUMO} (a.u.)	-0.0226	-0.0591	-0.0619	-0.0761	-0.0143	-0.0745	-0.0723
E_{HOMO} (eV)	-6.5634	-5.5566	-5.7307	-6.3401	-6.5960	-5.9919	-7.5402
E_{LUMO} (eV)	-0.6149	-1.6082	-1.6844	-2.0708	-0.3891	-2.0272	-1.9674
IΔE I = E_{HOMO}-E_{LUMO} gab (eV)	5.9457	3.9484	4.0436	4.2695	6.2069	3.9647	5.5729
Ionization potentials, I = - E_{HOMO} (eV)	6.5634	5.5566	5.7307	6.3401	6.5960	5.9919	7.5402
Electron affinity, A=-E_{LUMO} (eV)	0.6149	1.6082	1.6844	2.0708	0.3891	2.0272	1.9674
Chemical hardness, η = (I – A)/2 (eV)	2.9742	1.9741	2.0245	2.1361	3.1048	1.9837	2.7864
Chemical softness, S = 1/(2η) (eV)	0.1681	0.2533	0.2471	0.2342	0.1611	0.2522	0.1794
Electronegativity, χ = -(I + A)/2 (eV)	3.5892	3.5837	3.7089	4.2069	3.4939	4.0109	4.7538
Chemical potential, μ = - χ (eV)	-3.5892	-3.5837	-3.7089	-4.2069	-3.4939	-4.0109	-4.7538
Electrophilicity index, ω = $μ^2$/2η (eV^{-1})	2.1660	3.2502	3.3987	4.1416	1.9647	4.0545	4.0545

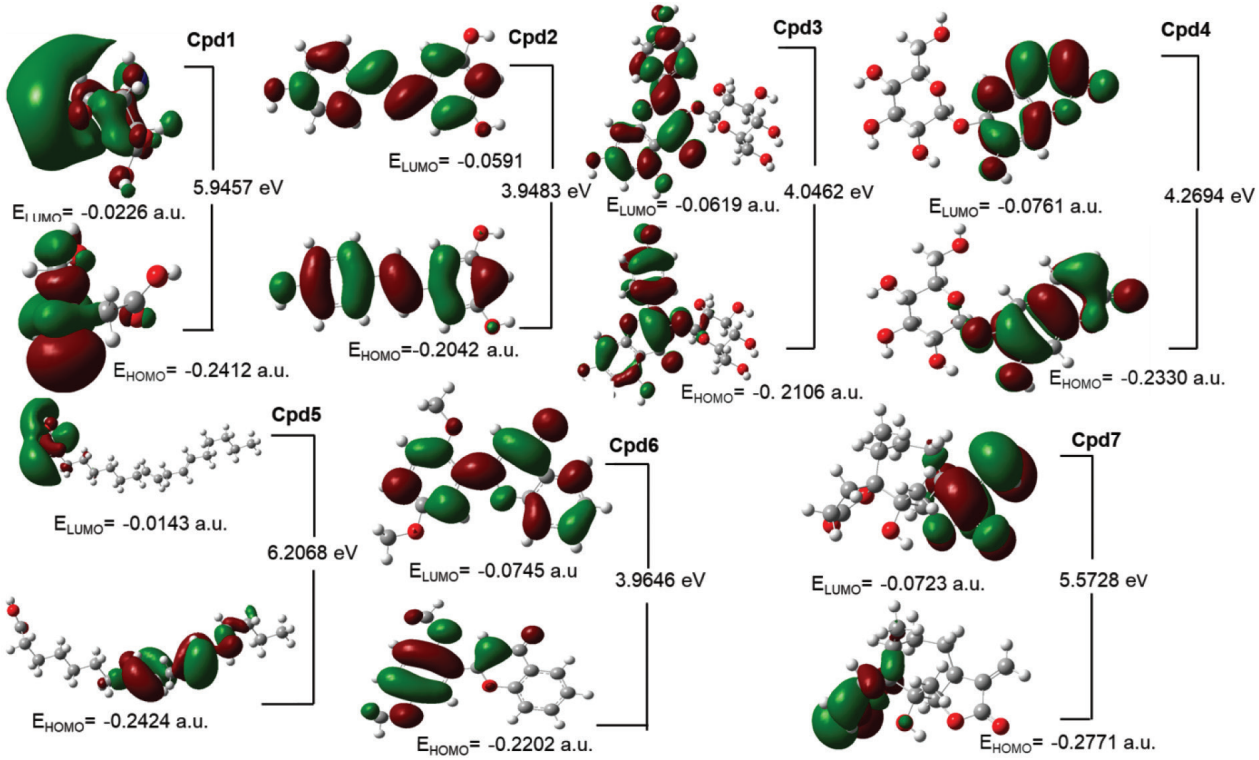

Figure 2. 3D HOMO and LUMO frontier orbitals of the (1–7) cpd compounds calculated at the B3LYP-31++G (d, p) level of theory.

as such, had a lower chemical hardness than those of the carboxylic acid-bearing compounds (1 and 5).

Molecular electrostatic potential (MEP) is a graphical representation employed to delineate the spatial distribution of electron density and the three-dimensional charge distribution in a molecule. The determination of charge distributions is crucial in assessing the strength of van der Waals interactions between molecules. MEP has been established as a valuable metric for elucidating hydrogen bonding and correlating reactivity with molecular structure (Murray and Politzer 2011, 2017). In order to align MEP with the molecular surface, we employed GaussView (Dennington et al. 2009) and used the optimized structures of the compounds depicted in Fig. 1. Fig. 3 presents a three-dimensional plot of the molecular electrostatic potential. The specific colors chosen in this instance are intended to depict regions of attractive potential in shades of red and yellow, which are indicative of electrophilic reactivity and correspond to the negative potential of MEP. Conversely, regions of repulsive potential are represented in blue, symbolizing nucleophilic reactivity and the positive potential of MEP, making them an ideal location for electrophilic attacks.

The MEP of cpd1 indicates a low electrostatic potential for the C=O bond and a high electrostatic potential for the hydrogen atoms in O-H bonds; thus, these hydrogen atoms behave like acceptors, whereas the hydrogen atom in the N-H bond is characterized by a relative abundance of electrons, so these bonds behave like donors.

The resulting overall MEP of cdp2 indicates that the oxygen atoms carrying protons are not attractive to the negative test charge. The MEP of cpd3 and cpd4 showed a relatively low potential and yellow color, characterized by a relatively abundant number of electrons at the oxygen atoms. The 3D plots of MEP for cpd5, cpd6, and cpd7 revealed that the oxygen atoms of the carbonyl group were subject to nucleophilic reactivity. In cpd5, the H atom in the O-H bond is characterized by the absence of electrons; therefore, this hydrogen atom behaves like an acceptor.

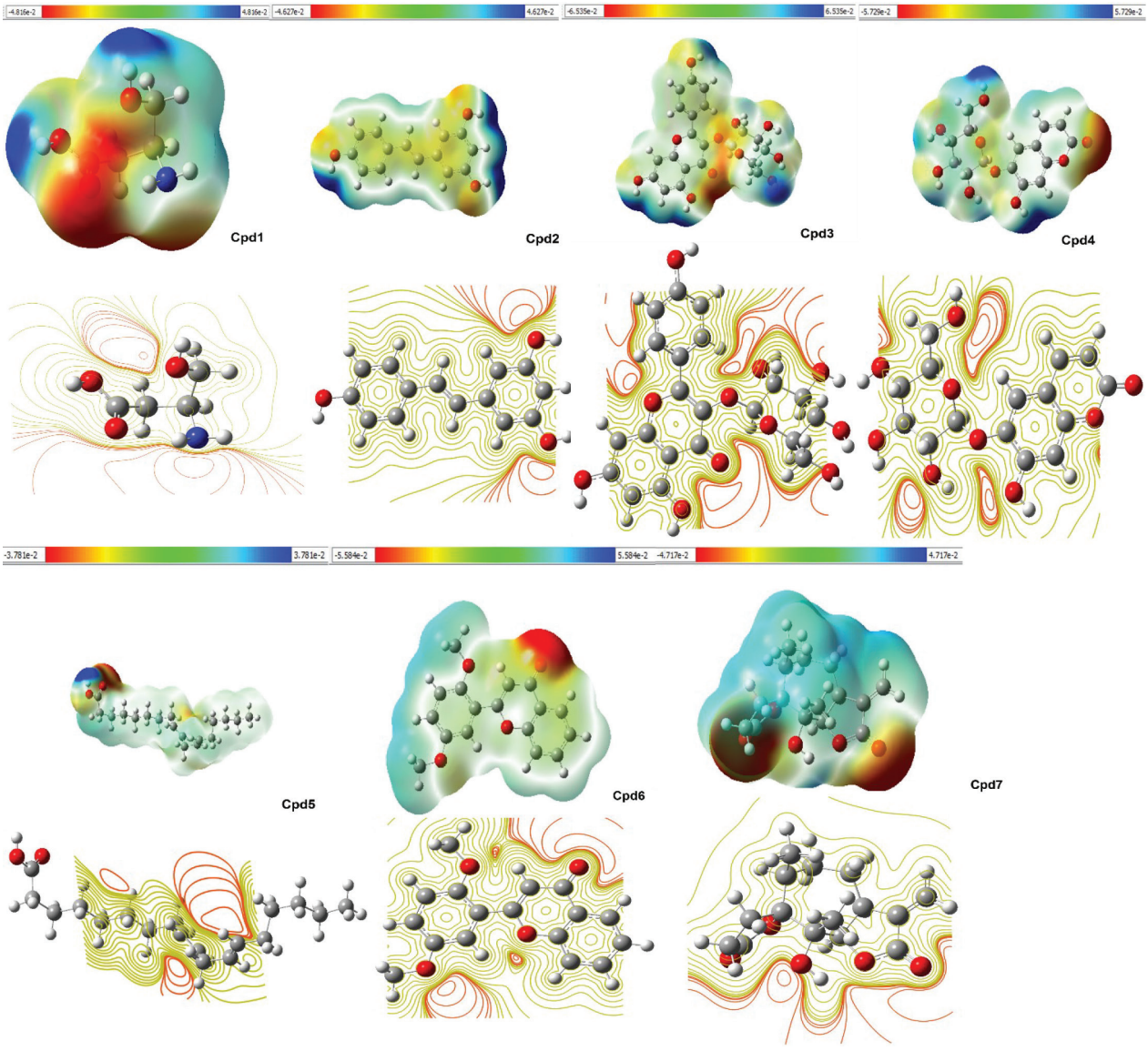

Figure 3. The 3D plot of the molecular electrostatic potentials (in a.u.) formed by mapping the total density and the corresponding contours of Cpd (1–7).

To observe all the MEP surfaces, we plotted each surface as a contour around the molecule. Fig. 3 shows surface contour plots for each molecule. Each contour curve around the molecule is the MEP surface; the outer contour has a lower isosurface value, whereas the inner contour has a higher isosurface value. This explanation is similar to that of the MEP for the selected contour.

Determination of QSPR

Following the DFT analysis, QSPR was used to correlate the physical parameters that can influence the clearance of the studied compound. QSPR analysis was conducted for the four compounds based only on their physicochemical properties, toxicity profile, and DFT analysis. The calculated chemical descriptors and QSPR results are summarized in Tables 4, 5, respectively.

The regression analysis identified the optimal regression equation for this study, which demonstrated the strongest correlation coefficients and significance values among the five equations examined. Specifically, the ideal regression equation was as follows (Widiyana et al. 2018):

$$\text{Log } 1/CL_{TOT} = 0.93\ E_{HOMO} + 6.90$$

Because it had the best correlation coefficient (R = 0.98), the smallest significance of 0.02 (0.05), the smallest standard error (SE = 0.12), and the highest F value (41.45), it was chosen (Table 4). Thus, the electronic parameter E_{HOMO} is the physical chemistry parameter that influences CL_{TOT}, according to the equation.

Table 4. Data on chemical descriptors.

Compounds	Lipophilic		Electronic		Steric	CL_{TOT}	Log (1/CL_{TOT})
	LogP	LogS	E_{HOMO}	E_{LUMO}	MW		
Kaempferol-3-O-glucoside	-0.65	-2.36	-5.7307	-1.6844	448.38	0.27	0.57
Esculin	-1.13	-1.11	-6.3401	-2.0708	340.28	0.80	0.10
Linoleic acid	5.45	-4.63	-6.5960	-0.3891	280.45	1.936	-0.28
2'-5-dimethoxy flavone	3.14	-4.28	-5.9919	-0.3891	282.29	0.33	0.47

LogP, partition coefficient; LogS: Solubility; E_{HOMO}: Highest occupied molecular orbital (eV); E_{LUMO}: Lowest unoccupied molecular orbital (eV); MW: Molecular weight (g/mol); CL_{TOT}, total clearance (log mL/min/kg).

Table 5. Regression analysis between physical and chemical properties with $1/CL_{TOT}$.

No.	Independent Variable	R	SE	F	Sig.	Equation
1	LogP	0.54	0.40	0.85	0.45	$\text{Log}1/CL_{TOT} = -0.06\ \text{LogP} + 0.33$
2	LogS	0.25	0.46	0.14	0.75	$\text{Log } 1/CL_{TOT} = 0.06\ \text{LogS} + 0.40$
3	E_{HOMO}	0.98	0.15	41.45	0.02	$\text{Log } 1/CL_{TOT} = 0.93\ E_{HOMO} + 6.90$
4	E_{LUMO}	0.34	0.41	2.54	0.73	$\text{Log } 1/CL_{TOT} = -0.15\ E_{LUMO} - 0.22$
5	MW	0.58	0.38	1.02	0.42	$\text{Log } 1/CL_{TOT} = 0.002\ \text{MW} - 0.75$

Molecular docking study

To clarify the interactions between proteins and ligands, a molecular docking study was performed to explore the binding modes of the isolated compounds and xanthine oxidase. Re-docking of quercetin in the active site of xanthine oxidase was used to test the accuracy of the docking process. In the absence of water molecules, Fig. 4 shows docked quercetin and co-crystallized quercetin in nearly identical positions among the receptors (RMSD = 0.39), confirming the validity of the docking process using the EP scoring function. Table 6 summarizes the findings of this study, including the predicted glide scores and the binding interactions of the docked compounds. The obtained results were consistent with those of the DFT analysis.

Molecular docking of all compounds revealed that Kaempferol-3-O-glucoside and Esculin gave the best glide scores (-8.391 and -10.184 kcal/mol, respectively), even more than the reference compound, with a binding score of -1.654 kcal/mol.

We noticed that the two compounds formed a hydrogen bond with the Glu802 residue as the binding of the reference ligand and the native ligand, which also formed other important hydrogen bonds with the residues Ser876 and Thr1010.

Esculin, which had the best docking score, formed two hydrogen bonds with the Glu802 residue and one hydrogen bond with each of the Lys771 and Ser876 residues. Moreover, it developed hydrophobic interactions and one aromatic π–π stacking interaction with Phe1013, which explains its high Glide score and binding energy (Fig. 5).

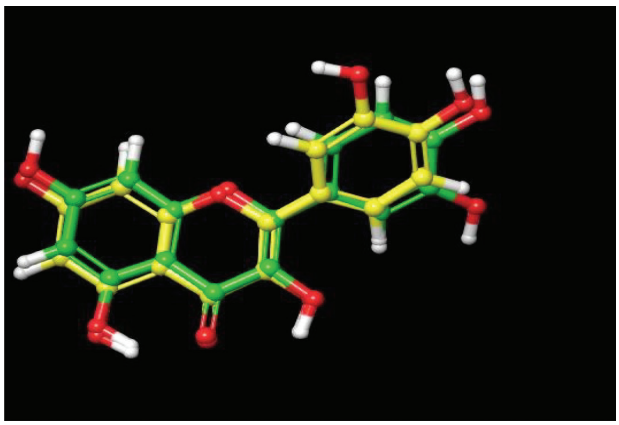

Figure 4. Docked (yellow colored) and co-crystallized quercetin (green colored) in the active side of Xanthine oxidase.

Table 6. Glide score and binding interactions of the promising compounds, reference standards, and native ligands.

Compound	Glide Score	H bonding	Pi-Pi stacking
Compd. 3	-8.391	**Glu 802**, Ser 876	Phe 1013
Compd. 4	-10.184	**Glu 802**, Lys 771, Ser 876	Phe 1013
Compd. 5	-7.099	**Glu 802**, Thr 1010	-
Compd. 6	-6.542	-	Phe 1009, Phe 914
Quercetin	-5.946	**Glu 802**, Ser 876, **Thr 1010**, **Arg 880**	Phe 1009, Phe 914
Oxypurinol	-1.654	**Glu 802, Arg 880**, Thr 1010	Phe 1009, Phe 914

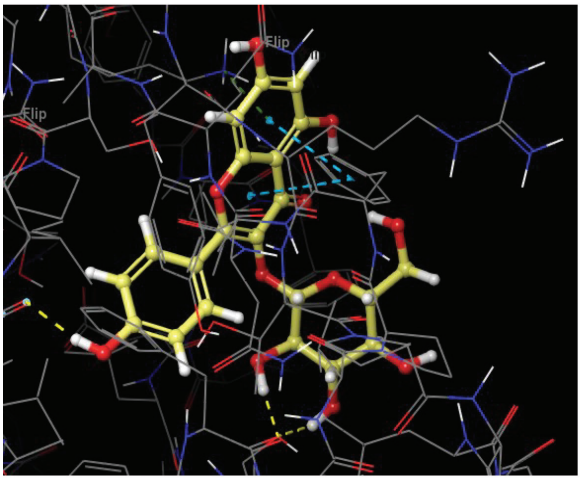

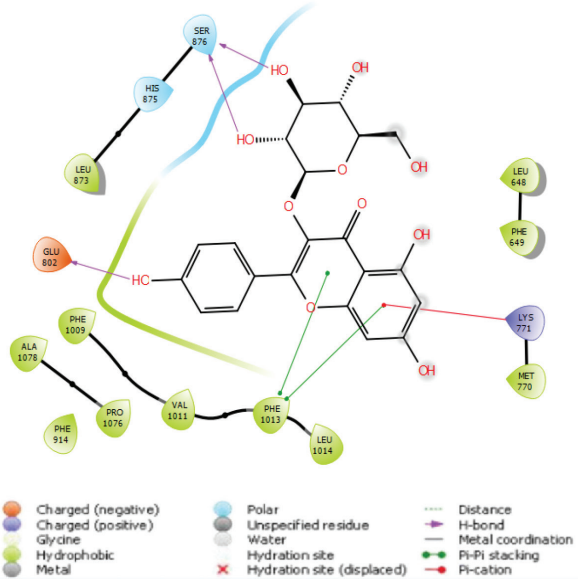

Compound 3

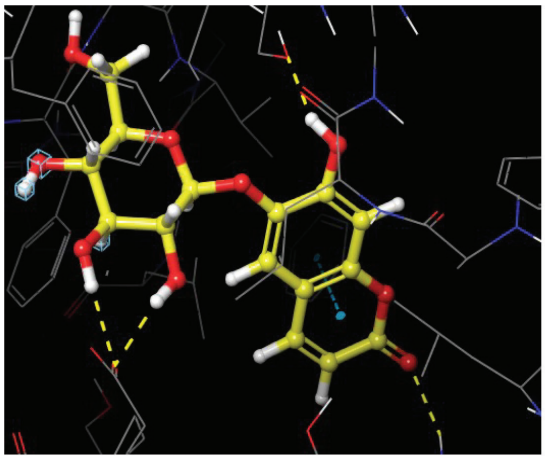

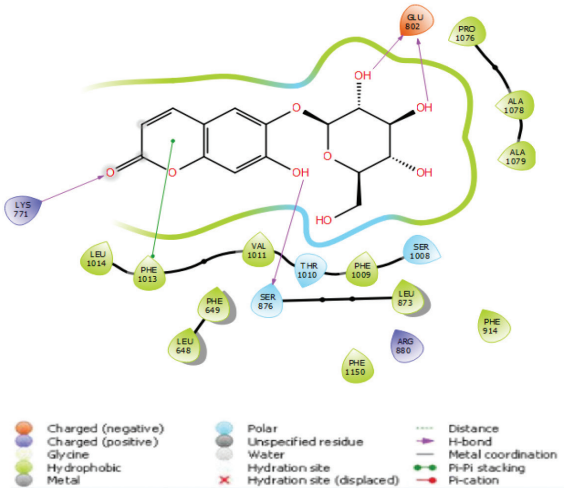

Compound 4

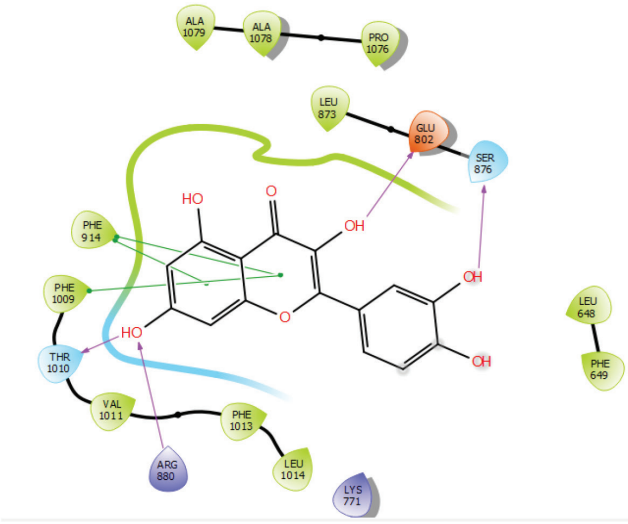

Quercetin

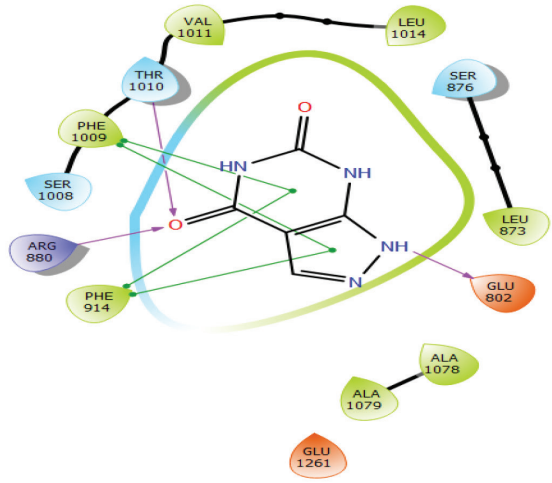

Oxypurinol

Charged (negative)
Charged (positive)
Glycine
Hydrophobic
Metal
Polar
Unspecified residue
Water
Hydration site
Hydration site (displaced)
Distance
H-bond
Metal coordination
Pi-Pi stacking
Pi-cation

Figure 5. 3D and 2D binding disposition of compounds 3, 5, reference standard, and native ligand after docking calculations in the active site of XO.

Kaempferol-3-O-glucoside showed significant stability at the active site, with a docking score that was higher than that of the reference ligand. It forms an important hydrogen bond with the Glu802 residue as well as two hydrogen bonds with the Ser876 residue. In addition, it developed different hydrophobic interactions and two aromatic π–π stacking interactions with Phe1013 (Fig. 5).

Conclusion

The results of this study validate and support the use of selected plants in Sudanese traditional medicine for the treatment of diseases caused by oxidative stress damage in the human body. From the in silico assessment of the compounds as XO inhibitors and their high inhibitory interactions, physicochemical properties, and structural analysis, Kaempferol-3-O-glucoside and Esculin have been suggested as possible natural drugs against certain diseases related to increased levels of XO. Therefore, further studies are recommended for in vitro and in vivo assessments as potent inhibitors, in addition to in vivo toxicity studies.

Authors' credit statements

S.S. conducted the computational analysis and wrote the manuscript draft; S.A. and Y.U. conducted the DFT analysis; N.M. isolated the compounds; and W.O. and M.M. revised the manuscript. K. E. conducted the docking study; A.A., A.S., and W.O. drafted the manuscript. A. A. and A. S. funded the study and revised the manuscript. All authors approved the final draft of the manuscript.

Availability of data and materials

The datasets generated and/or analyzed during the current study are available in the manuscript and UniProt (https://www.uniprot.org/) with accession number P47989.

Funding

This study was supported by funding from Prince Sattam bin Abdulaziz University project number (PSAU/2024/R/1445).

References

Ahmane N, Atmani-Kilani D, Chaher N, Ayouni K, Rahmani-Berboucha M, Costa GDA, Debbache-Benaida N, Richard T, Atmani D (2019) Identification of bioactive compounds from *Fraxinus angustifolia* extracts with anti- NADH oxidase activity of bovine milk xanthine oxidoreductase. Turkish Journal of Biology 5(43): 133–147. https://doi.org/10.3906/biy-1810-26

Becke AD (1993) Density functional thermochemistry-III. The role of exact exchange. The Journal of Chemical Physics 98: 5648–5652. https://doi.org/10.1063/1.464913

Bergström CAS, Charman WN, Porter CJH (2016) Computational prediction of formulation strategies for beyond-rule-of-5 compounds. Advanced Drug Delivery Reviews 101: 6–21. https://doi.org/10.1016/j.addr.2016.02.005

Borges F, Fernandes E, Roleira F (2002) Progress towards the discovery of xanthine oxidase inhibitors. Current Medicinal Chemistry 9(2): 195–217. https://doi.org/10.2174/0929867023371229

Dennington R, Keith T, Millam J (2009) Gauss View, Version 5. Semichem Inc., Shawnee Mission.

Dhiman R, Sharma S, Singh G, Nepali K, Singh Bedi PM (2013) Design and synthesis of aza-flavones as a new class of xanthine oxidase inhibitors. Arch Pharm (Weinheim) 346(1): 7–16. https://doi.org/10.1002/ardp.201200296

El-Naeem A, Abdalla S, Ahmed I, Alhassan G (2022) Phytochemicals and in silico investigations of Sudanese roselle. South African Journal of Science 118(1/2). https://doi.org/10.17159/sajs.2022/10383

Frisch MJ, Trucks G, Schlegel HB, Scuseria GE, Robb MA, et al. (2009) Gaussian 09, Revision A.02, Gaussian, Inc., Wallingford CT.

Gunasekaran S, Balaji RA, Kumeresan S, Anand G, Srinivasan S (2008) Experimental and theoretical investigations of spectroscopic properties of N-acetyl-5-methoxytryptamine. Canadian Journal of Analytical Sciences and Spectroscopy 53: 149–160.

Habtemariam S (2011) A-glucosidase inhibitory activity of kaempferol-3-O-rutinoside. Natural Product Communications 6(2): 201–203.[PMID:21425674]https://doi.org/10.1177/1934578X1100600211

Hediger MA, Johnson RJ, Miyazaki H, Endou H (2005) Molecular physiology of urate transport. Physiology 20: 125–133. https://doi.org/10.1152/physiol.00039.2004

Helal E, Abou-Aouf N, Khattab S, Meselhy A, Abu-Amara T (2014) The Effects of *Ambrosia maritima*, L. (Damsissa) on Some Biochemical and Histological Parameters of Diabetic Albino Rats. The Egyptian Journal of Hospital Medicine 57(1): 612–629. https://doi.org/10.12816/0008492

Hosoya T, Kimura K, Itoh S, Inaba M, Uchida S, Tomino Y, Makino H, Matsuo S, Yamamoto T, Ohno I, Shibagaki Y, Iimuro S, Imai N, Kuwabara M, Hayakawa H (2014) The effect of febuxostat to prevent a further reduction in renal function of patients with hyperuricemia who have never had gout and are complicated by chronic kidney disease stage 3: study protocol for a multicenter randomized controlled study. Trials 15: 26. https://doi.org/10.1186/1745-6215-15-26

Kumar R, Kumar D, Sharma S, Singh R (2011) Xanthine oxidase inhibitors: a patent survey. Expert Opinion on Therapeutic Patents 21(7): 1071–1108. https://doi.org/10.1517/13543776.2011.577417

Kurt M, Babu PC, Sundaraganesan N, Cinar M, Karabacak M (2011) Molecular structure, vibrational, UV and NBO analysis of 4-chloro-7-nitrobenzofurazan by DFT calculations. Spectrochimica Acta Part A 79: 1162–1170. https://doi.org/10.1016/j.saa.2011.04.037

Lee C, Yang W, Parr RG (1988) Development of the Colic-Salvetti correlation-energy formula into a functional of the electron density. Physical Review B 37: 785–788. https://doi.org/10.1103/PhysRevB.37.785

Lü JM, Yao Q, Chen C (2013) 3,4-Dihydroxy-5-nitrobenzaldehyde (DHNB) is a potent inhibitor of xanthine oxidase: a potential therapeutic agent for treatment of hyperuricemia and gout. Biochemical

Pharmacology 86(9): 1328–1337. https://doi.org/10.1016/j.bcp.2013.08.011

Mehmood A, Ishaq M, Zhao L, Safdar B, Rehman AU, Munir M, Raza A, Nadeem M, Iqbal W, Wang C (2019) Natural compounds with xanthine oxidase inhibitory activity: A review. Chemical Biology & Drug Design 93(4): 387–418. https://doi.org/10.1111/cbdd.13437

Mohamed NS, Mohamed MS, Mothana RA, Osman WJ, Khalid HS (2020) HPTLC fingerprint profiles and UPLC-MS identification of potential antioxidant fractions and compounds from *Ambrosia maritima* L. and *Ammi majus* L. African Journal of Biotechnology 19(5): 249–258. https://doi.org/10.5897/AJB2020.17114

Mohamed Isa SSP, Ablat A, Mohamad J (2018) The antioxidant and xanthine oxidase inhibitory activity of *Plumeria rubra* Flowers. Molecules 23(2): 400. https://doi.org/10.3390/molecules23020400

Murray JS, Politzer P (2011) The electrostatic potential: an overview.Computational Molecular Science 1: 153–163. https://doi.org/10.1002/wcms.19

Murray JS, Politzer P (2017) Molecular electrostatic potentials and noncovalent interactions. Computational Molecular Science 7: 1–10. https://doi.org/10.1002/wcms.1326

Naqvi BS, Shaikh MR, Maleka FA, Shaikh D (1994) Studies of antibacterial activity of ethanolic extracts from *Nericumindicum* and *Habiscus rosasinensis*. Journal of Islamic World Academy of Sciences 7: 167–168. https://jag.journalagent.com/ias/pdfs/IAS_7_3_167_168.pdf

Nepali K, Agarwal A, Sapra S, Mittal V, Kumar R, Banerjee UC, Gupta MK, Satti NK, Suri OP, Dhar KL (2011) N-(1,3-Diaryl-3-oxopropyl) amides as a new template for xanthine oxidase inhibitors. Bioorganic & Medicinal Chemistry 19(18): 5569–5576. https://doi.org/10.1016/j.bmc.2011.07.039

Niu X, Wang Y, Li W, Zhang H, Wang X, Mu Q, He Z, Yao H (2015) Esculin exhibited anti-inflammatory activities in vivo and regulated TNF-α and IL-6 production in LPS-stimulated mouse peritoneal macrophages in vitro through MAPK pathway. International Immunopharmacology 29(2): 779–786. https://doi.org/10.1016/j.intimp.2015.08.041

OECD [Organisation for Economic Co-Operation and Development] (2001) Guideline for Testing of Chemicals. OECD.

Pacher P, Nivorozhkin A, Szabó C (2006) Therapeutic effects of xanthine oxidase inhibitors: renaissance half a century after the discovery of allopurinol. Pharmacological Reviews 58(1): 87–114. https://doi.org/10.1124/pr.58.1.6

Pires DE, Blundell TL, Ascher DB (2015) pkCSM: Predicting Small-Molecule Pharmacokinetic and Toxicity Properties Using Graph-Based Signatures. Journal of Medicinal Chemistry 58(9): 4066–4072. https://doi.org/10.1021/acs.jmedchem.5b00104

Radi R, Rubbo H, Bush K, Freeman BA (1997) Xanthine oxidase binding to glycosaminoglycans: kinetics and superoxide dismutase interactions of immobilized xanthine oxidase-heparin complexes. Archives of Biochemistry and Biophysics 339(1): 125–135. https://doi.org/10.1006/abbi.1996.9844

Said TMA, Elgasim EA, Eltilib HHAB, Bekhit AEDA, Al-Juhaimi FY, Mohamed Ahmed IA (2018) Antioxidant and antimicrobial potentials of Damsissa (*Ambrosia maritima*) leaf powder extract added to minced beef during cold storage. CyTA – Journal of Food 16(1): 642–649. https://doi.org/10.1080/19476337.2018.1448456

Schrodinger (2021) Schrodinger Release 2021-4. Glide, Schrodinger, LLC, New York, NY.

Shoombuatong W, Prathipati P, Prachayasittikul V, Schaduangrat N, Malik AA, Pratiwi R, Wanwimolruk S, Wikberg JES, Gleeson MP, Spjuth O, Nantasenamat C (2017) Towards Predicting the Cytochrome P450 Modulation: From QSAR to Proteochemometric Modeling. Current Drug Metabolism 18(6): 540–555. https://doi.org/10.2174/1389200218666170320121932

Srimai V, Ramesh M, Parameshwar KS, Parthasarathy T (2013) Computer-aided design of selective cytochrome P450 inhibitors and docking studies of alkylresorcinol derivatives. Medicinal Chemistry Research 22: 5314–5323. https://doi.org/10.1007/s00044-013-0532-5

Sousa S. F., Fernandes P.A, Ramos M. J. (2007) General performance of density functionals. Journal of Physical Chemistry A111: 10439–10452. https://doi.org/10.1021/jp0734474

Spector T, Johns DG (1970) Stoichiometric inhibition of reduced xanthine oxidase by hydroxypyrazolo [3,4-d]pyrimidines. The journal of Biological Chemistry 245(19): 5079–6085. https://doi.org/10.1016/S0021-9258(18)62820-0

Testa B, Kraemer SD (2007) The biochemistry of drug metabolism an introduction testa chemistry & biodiversity. Chemistry & Biodiversity 4(3). https://doi.org/10.1002/cbdv.200790032

Wang Y, Tang C, Zhang H (2015) Hepatoprotective effects of kaempferol 3-O-rutinoside and kaempferol 3-O-glucoside from *Carthamus tinctorius* L. on CCl_4-induced oxidative liver injury in mice. Journal of Food and Drug Analysis 23(2): 310–317. https://doi.org/10.1016/j.jfda.2014.10.002

Widiyana AP, Putra GS, Muchlashi LA, Sulistyowaty MI, Budiati T (2018) Design and molecular docking studies of quinazoline derivatives as antiproliferation. Jurnal Farmasi Dan Ilmu Kefarmasian Indonesia 3(2): 44–48. https://doi.org/10.20473/jfiki.v3i22016.44-48

Xu H, Li C, Mozziconacci O, Zhu R, Xu Y, Tang Y, Chen R, Huang Y, Holzbeierlein JM, Schöneich C, Huang J, Li B (2019) Xanthine oxidase-mediated oxidative stress promotes cancer cell-specific apoptosis. Free Radical Biology and Medicine 139: 70–79. https://doi.org/10.1016/j.freeradbiomed.2019.05.019